

Chiral topological phases and fractional domain wall excitations in one-dimensional chains and wires

Jukka I. Väyrynen and Teemu Ojanen*

Low Temperature Laboratory, Aalto University, P. O. Box 15100, FI-00076 AALTO, Finland

(Dated: December 26, 2018)

According to the general classification of topological insulators, there exist one-dimensional chirally (sublattice) symmetric systems that can support any number of topological phases. We introduce a zigzag fermion chain with spin-orbit coupling in magnetic field and identify three distinct topological phases. Zero-mode excitations, localized at the phase boundaries, are fractionalized: two of the phase boundaries support $\pm e/2$ charge states while one of the boundaries support $\pm e$ and neutral excitations. In addition, a finite chain exhibits $\pm e/2$ edge states for two of the three phases. We explain how the studied system generalizes the Peierls-distorted polyacetylene model and discuss possible realizations in atomic chains and quantum spin Hall wires.

PACS numbers: 73.43.-f, 73.63.Hs, 85.75.-d

Introduction– The discovery of quantum spin Hall effect in two dimensional electron systems initiated an enormous wave of research exploring topological properties of gapped band structures [1, 2]. This has led to various recent discoveries of novel states of matter, commonly known as topological insulators, exhibiting striking properties such as exotic electromagnetic responses and gapless surface states [3]. The quest for novel topological insulators, guided by the comprehensive classification presented in Ref. [4], is one of the most active topics in condensed matter physics at the moment.

In one spatial dimension (1D) the recent attention has concentrated on the topological superconducting phases realized in spin-orbit coupled semiconductor nanowires in proximity of a superconductor [5, 6]. It was proposed that networks of wires could serve as a platform for topological quantum computation [7]. However, the study of topological phases in 1D systems can be traced back over 30 years to the discovery of soliton excitations in polyacetylene [8]. Indeed, the Su-Schrieffer-Heeger model is an example of an insulator exhibiting a chiral symmetry [9]. The zero-energy states located between differently dimerized domains support neutral spin-1/2 excitations and spinless $\pm e$ excitations.

In this work we introduce a zigzag fermion chain model with a spin-orbit coupling in a magnetic field. This system belongs to the BDI class in the classification scheme and has three distinct topological phases depending on the orientation and magnitude of the magnetic field. The domain wall (DW) excitations localized at the phase boundaries are fractionalized: two of the DWs support a single zero mode with possible charge states $\pm e/2$ while one DW supports two zero modes leading to $\pm e$ and neutral excitations. Furthermore, a finite chain exhibits $\pm e/2$ charged edge states for two of the three phases. The most striking differences to the polyacetylene model include existence of three distinct phases (instead of two) and possibility to realize $\pm e/2$ excitations that are absent in polyacetylene due to spin degeneracy. Zigzag

chains are realized in a number of systems which indicates that the studied model could be relevant, for example, in monoatomic gold chains in magnetic fields. Additionally, a continuum limit of the considered model describes narrow wires of quantum spin Hall insulators. Interestingly, in this case the $\pm e/2$ excitations can be thought of as a bound pairs of $\pm e/4$ charges on opposite edges of the wire.

1D models and phase diagrams– In strictly 1D chains the Peierls instability commonly results in geometrical deformations doubling the unit cell and creating a sublattice structure. If atoms are not restricted to a line, chains can relax to planar zigzag or more complicated structures. Motivated by this, we consider a zigzag fermion chain shown in Fig. 1a. The Hamiltonian of the system is

$$H = t \sum_{\langle i,j \rangle} c_i^\dagger c_j + \delta \sum_{\langle\langle i,j \rangle\rangle} (-1)^i c_i^\dagger c_j + i \frac{\lambda}{|e_{ij}|} \sum_{\langle\langle i,j \rangle\rangle} c_i^\dagger \mathbf{S} \cdot \mathbf{e}_{ij} c_j + \sum_i c_i^\dagger \mathbf{m} \cdot \mathbf{S} c_i \quad (1)$$

where the first term describes the nearest-neighbor hopping and the second term encodes the hopping modulation due to dimerization. The third term arises from the next-nearest neighbor spin-orbit hopping and the last term corresponds to the Zeeman splitting $\mathbf{m} = (m_x, m_y)$ due to the external magnetic field. The spin-orbit term depends on the orientation of the two bonds connecting the next-nearest neighbors $\mathbf{e}_{ij} = \mathbf{d}_i \times \mathbf{d}_j$ and vanishes for strictly linear chains [1]. The spin-orbit coupling and magnetization are crucial for the studied topological properties of the system while the hopping modulation is included for the sake of generality. The model (1), with an in-plane magnetic field leads to the Bloch Hamiltonian

$$H(k) = 2t \cos(ka) \sigma_x + 2\delta \sin(ka) \sigma_y + 2\lambda \sin(2ka) \sigma_z S_z + m S_x \quad (2)$$

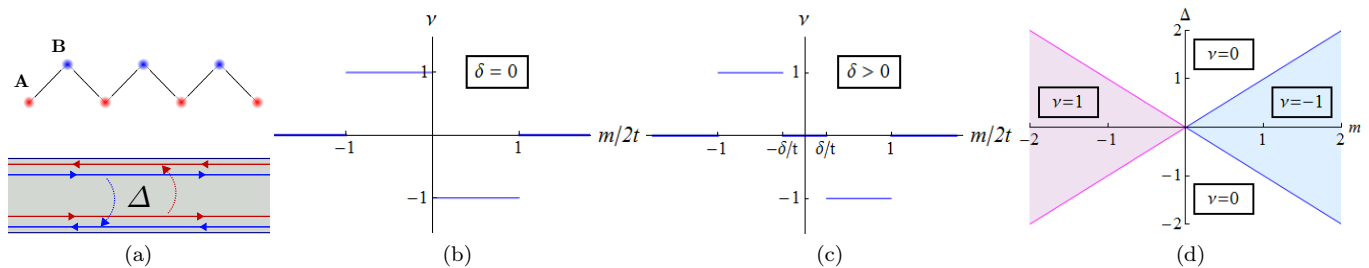


Figure 1: (a) Studied 1D models, a zigzag fermion chain with a spin-orbit hopping and narrow quantum spin Hall wire with a finite inter-edge coupling. Topological properties of these systems are closely related. (b–d) The phase diagrams of Hamiltonians (2) and (4) as a function of model parameters. (b) For vanishing hopping modulation $\delta = 0$ there is a $(1/-1)$ interface at $m = 0$. (c) For a finite δ , a trivial phase emerges for $|m| < |\delta|$. (d) The Hamiltonian (4) shows three different phases for finite inter-edge coupling Δ . The normalization of (3) is multiplied by 2 since continuum models produce half-integer values.

where Pauli matrices σ_i and S_i operate in the sublattice and spin space, respectively. The Hamiltonian (2) possesses a chiral symmetry: it anticommutes with $C = \sigma_z S_y$. This property has important consequences on the energy spectrum and topological properties of the system [4]. If H has an eigenstate $|E_i^+\rangle$ with energy E_i , there exists another eigenstate $C|E_i^+\rangle$ belonging to the energy $-E_i$, so the spectrum is symmetric about $E = 0$. Zero modes, if existing, can be chosen to coincide with the eigenstates of the generator of the chiral symmetry, $C|\psi^\pm\rangle = \pm|\psi^\pm\rangle$. In odd spatial dimensions systems with a chiral symmetry may possess topologically nontrivial phases characterized by a Z -valued topological index introduced in Ref. [4]. Here we employ alternative but equivalent formulation [10]. In 1D the invariant takes the form

$$\nu[H] = \frac{1}{8\pi i} \int dk \text{Tr} [CH^{-1}\partial_k H], \quad (3)$$

where the integration extends over the Brillouin zone for Bloch Hamiltonians and over the real line for continuum models.

In Fig. 1 we plot the invariant (3) for Hamiltonian (2) as a function of the magnetic field, revealing the phase diagram. The system has three distinct phases $\nu = \pm 1$ and $\nu = 0$, separated by quantum phase transitions. In these interfaces where the invariant changes its value, there exist zero energy states protected by the chiral symmetry. The phase of the system depends on m and can thus be changed by tuning the magnitude of the external field, i.e., by introducing magnetic DWs into the system. At large field values ($|m| > 2t$) the magnetization dominates and $\nu = 0$. We will show below that this phase can be identified with vacuum.

At vanishing spin-orbit coupling $\lambda = 0$ and magnetization $\mathbf{m} = 0$, model (2) describes a Peierls-distorted polyacetylene chain [8]. The resulting Hamiltonian anticommutes with $C' = \sigma_z$ which serves as the generator

of the chiral symmetry. Evaluation of the invariant (3) reveals two distinct topological phases with $\nu = \text{sign } \delta$. These phases correspond to the well-known degenerate dimer configurations of the chain. There is, however, important differences between the polyacetylene model and the zigzag chain. In polyacetylene there is no $\nu = 0$ phase which in our model is identified with vacuum. As a consequence, a finite polyacetylene chain does not exhibit robust edge states unlike $\nu = \pm 1$ zigzag chains. In addition, due to the spin degeneracy in polyacetylene, there are always two zero modes at phase boundaries. As we emphasize below, due to this fact the zigzag chain exhibits fractional domain wall charges $\pm e/2$ whereas polyacetylene has $\pm e$ and neutral excitations.

There is an interesting connection between the model (2) and quantum spin Hall (QSH) wires (Fig. 1a). A QSH bar supports helical edge states where the velocity and spin of the edge carriers are completely correlated [3]. In a narrow enough wire the edge modes localized on opposite edges begin to overlap, enabling interedge hybridization which gaps the edge spectrum. The Hamiltonian describing the systems is

$$H(k) = v_F k \sigma_z S_z + \Delta \sigma_x + m S_x, \quad (4)$$

where the first term describes the unperturbed edge states, the second term comes from the inter-edge tunneling and the last term corresponds to magnetization. The Pauli matrices σ now operate in the subspace of the two edges of the wire. Setting $\delta = 0$ and expanding the band Hamiltonian (2) around $k = 0$ or $k = \pi$, and identifying $2t \rightarrow \Delta$ and $4\lambda a \rightarrow v_F$, one recovers (4). The close connection between (2) and (4) suggests that the topological properties of these systems bear similarities. The phase diagram of (4), shown in Fig. 1d, reveals three distinct phases as a function of the relevant control parameters Δ and m . The zero-energy states at DWs are also very similar to those of the zigzag chain as we explain below.

Zero modes and fractional excitations— Now we analyze

zero modes by numerical diagonalization of the lattice model and analytical methods and identify associated quantum numbers. As mentioned above the spectrum is symmetric with respect to $E = 0$. This property and the number of the zero modes at DWs are sufficient to determine the charge states of the zero mode excitations [8, 11]. According to the general argument, one-half of an electron state per zero mode is missing from the valence band in the vicinity of a DW. If a DW supports a single zero mode, then the possible charge states at half filling are $\pm e/2$ depending on the population of the zero mode. If there exist two zero modes, possible charge states are $\pm e$ and 0. The total energy of the system is independent of the population of the zero modes. In finite systems where the DWs come in pairs zero modes are split to linear combinations of $|\psi^\pm\rangle$ with finite energies around $E = 0$, approaching zero as the separation of the DWs increases.

At the DWs where the phase $\nu = 1$ changes to $\nu = 0$ (referred as the 1/0 DW) we solve the model (1) in a finite ring with spatially varying magnetization m . For simplicity we assume that $\delta = 0$ in this section, so there are two phase boundaries located at places where m crosses $2t$. We choose a magnetization profile so that the DWs occur at the opposite sides of the ring. As illustrated in Fig. 2a, we discover two mid-gap energy states, both located at the DWs. When the ring size is increased the energies move closer to zero and eventually become degenerate. This result can be complemented by an analytical calculation based on the continuum approximation of Eq. (2). Linearizing (2) at Brillouin zone point $k = 0$ (or π) where the gap closes, we solve the Schrödinger equation for zero energy states. We find one normalizable solution $\psi_{1/0}(x)$ ($\psi_{0/1}(x)$) located at a DW (anti-DW),

$$\begin{aligned}\psi_{1/0}(x) &= A e^{\int_{x_0}^x dx' \frac{2t+m(x')}{4\lambda a}} |a^+\rangle \\ \psi_{0/1}(x) &= A e^{-\int_{x_0}^x dx' \frac{2t+m(x')}{4\lambda a}} |a^-\rangle\end{aligned}\quad (5)$$

where $|a^\pm\rangle = (|\uparrow\rangle|y_\pm\rangle + |\downarrow\rangle|y_\mp\rangle)$ and $|\uparrow, \downarrow\rangle, |y_\pm\rangle$ denote the eigenstates of σ_z and S_y . The DW profile is determined by $m(x)$. For $\psi_{1/0}$ ($\psi_{0/1}$) $m(x)$ is an arbitrary decreasing (increasing) non-vanishing function satisfying $m(x_0) = -2t$ and approaching constant value away from x_0 . The normalization constant A is determined by the detailed form of $m(x)$. According to the general argument, there is a charge aggregate of $\pm e/2$ localized at the DW depending on whether the zero mode is populated ($-e/2$) or not ($e/2$) [8]. Since the total number of electrons must be an integer, the DWs must come in "soliton-antisoliton" pairs which is clear in the ring geometry. In a finite linear chain in the phase $\nu = \pm 1$ terminated by hard-wall boundary conditions we discover one zero mode at each end of the chain. Thus the terminated end behaves like the $\pm 1/0$ interface and supports $\pm e/2$ excitations. A finite chain in the phase $\nu = 0$ does

not exhibit mid-gap states, indicating that the $\nu = 0$ phase can indeed be identified with the vacuum. The corresponding DW states for model (4) can be obtained from Eq. (5) by substituting $2t \rightarrow \Delta$ and $4\lambda a \rightarrow v_F$. The $-1/0$ DW behaves similarly to the $1/0$ DW and does not require a separate treatment.

In contrast to $\pm 1/0$ DWs, a $-1/1$ DW supports two zero modes. The numerical diagonalization reveals four mid-gap states (two per DW) approaching zero energy as the ring size is increased. The wavefunctions of these states are localized at the DWs. Analytical approximation for the wavefunctions are obtained by linearizing (2) around $k = \pi/2$ and solving DW $\psi_{1/-1}(x)$ and anti-DW $\psi_{-1/1}(x)$ states

$$\begin{aligned}\psi_{-1/1}(x) &= A_\pm e^{\int_{x_0}^x dx' m(x') \frac{-2t \pm 4\lambda}{a((2t)^2 + (4\lambda)^2)}} |b^\pm\rangle \\ \psi_{1/-1}(x) &= B_\pm e^{\int_{x_0}^x dx' m(x') \frac{2t \pm 4\lambda}{a((2t)^2 + (4\lambda)^2)}} |c^\pm\rangle,\end{aligned}\quad (6)$$

where $|b^\pm\rangle = (|\uparrow\rangle|y_+\rangle \mp |\downarrow\rangle|y_-\rangle)$, $|c^\pm\rangle = (|\uparrow\rangle|y_-\rangle \pm |\downarrow\rangle|y_+\rangle)$. For $-1/1$ DW ($1/-1$) $m(x)$ is increasing (decreasing) function satisfying $m(x_0) = 0$ and approaching constant value away from x_0 . Since there are two zero modes per DW (anti-DW), the possible charge states are, as in polyacetylene, $\pm e$ and 0 depending whether both of the states are empty (e), one of them is excited (0) or both are excited ($-e$). In the case of an antisymmetric DM $m(x - x_0) = -m(x_0 - x)$ the valence band is spin paired so $\pm e$ charge states are actually spinless as in polyacetylene [8]. The argument for DW charge states is supported by calculations based on a method introduced in Ref. [12] recently. After an appropriate regularization, the DW charge (modulo multiples of e) follows from the expression

$$q = \frac{e}{4\pi^2} \int_{-\infty}^{\infty} dx \int_{-\infty}^{\infty} d\omega \int dk \mathcal{G} \partial_k \mathcal{G}^{-1} \mathcal{G} \partial_\omega \mathcal{G}^{-1} \mathcal{G} \partial_x \mathcal{G}^{-1}$$

where $\mathcal{G} = (i\omega - H(k, x))^{-1}$ is the Wigner transformed Green function [9, 12]. To extract DW charge, we will use the continuum approximation of H in the vicinity of the DW. Evaluation of the DW charge formula confirms that possible charges states for a $\pm 1/0$ DW ($-1/1$) are half-integral (integral) multiples of e .

The possible charge states of $1/0$ and $1/-1$ DWs coincide with spinless and spinfull polyacetylene DWs. However, the corresponding wavefunctions are quite different from those of polyacetylene zero modes, where DW and anti-DW wavefunctions are nonzero only on separate sublattices [8]. In our model the sublattice and spin structure follows directly from the property $C|\psi^\pm\rangle = \pm|\psi^\pm\rangle$, where the different signs correspond to DW and anti-DW zero modes. Our numerical calculations indicate that mid-gap states are insensitive to even-odd variation in the number of lattice sites and robust against weak disorder in system parameters.

Physical realizations— Zigzag fermion chains are known to exist in various physical contexts. Structurally the

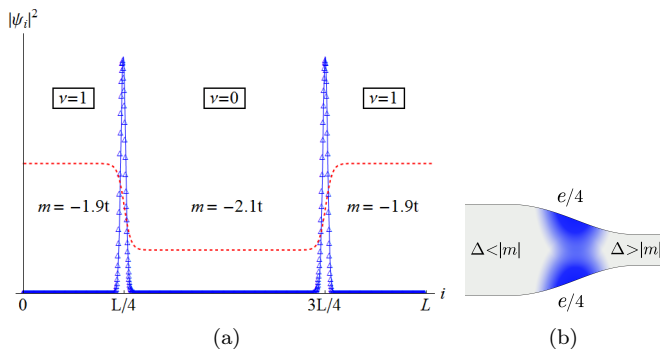


Figure 2: (a) Numerical solution of zero mode wavefunctions (blue triangles) for a ring with $L = 1200$ sites, $\lambda/t = 1/8$ and an analytical approximation based on continuum solutions (5). The red dashed line represents the magnetization profile. (b) In QSH wires a $1/0$ DW supports a fractional charge state $\pm e/2$ distributed evenly between $\pm e/4$ charges.

most closely related examples are monoatomic Au, Pt, and Ir chains [13, 14]. For example, Au spontaneously forms zigzag chains with one s-type conduction electron per site. Since spin-orbit effects are pronounced in heavy elements, these metal chains could provide a realization of the studied phenomenon. The exact shape of these structures, magnitude of the spin-orbit hopping λ and the g -factor determining m depend on the details of the system and are not readily available. Thus it is difficult to give a realistic estimate for the energy gap setting the relevant temperature scale. However, if our model captures the essential physics for these systems, a finite chain exhibits $\pm e/2$ edge states for any finite λ and $|m| < 2t$ at low temperatures.

More concrete estimates can be given for the QSH nanowire model (4) which has similar topological properties. In a thin wire the edge states on opposite edges have a weak overlap, inducing a gap Δ in the edge spectrum (4). This gap depends sensitively on the width of the wire [16] and can be engineered by modulating it. Magnetic field can be employed to tune the magnetization m [15] so by varying m and Δ it is possible to drive the system to different phases illustrated in Fig. 1d. In Ref. [16] it was estimated that for wires of width 200 nm the inter-edge coupling is $\Delta = 5.22$ K, while in Ref. [15] it was concluded that in-plane magnetization of $m = 3.5$ K can be realized by magnetic fields of the order 1T. These values suggest that experimental investigation of the phase diagram and the zero mode excitations of QSH wires is possible within existing methods at sub-Kelvin temperatures and high magnetic fields. As discussed in Ref. [15], the single-flavor Dirac spectrum realized in the edges of QSH systems have $\pm e/2$ excitations located at magnetic DWs. In a QSH wire the $\pm 1/0$ phase boundary realizes another exotic possibility, bound pairs of $\pm e/4$ charges on

opposite sides of the wire, as illustrated in Fig. 2b. The zero modes (6) are localized equally in both sublattices indicating that equal charges reside on opposite edges of the wire. Since the total charge on a DW is $\pm e/2$, opposite edges must have equal charges $\pm e/4$. The $\pm 1/0$ DW is taking place when magnetization and tunneling are equal, determining the critical width of the wire. In the narrow (wide) part of the wire tunneling can be made stronger (weaker) than the magnetization, resulting in the $0/1$ DW when the wire width exceeds the critical width. Unlike $e/2$ charges studied in [15], $e/4$ charges rely on inter-edge coupling and are inherently bound together. The maximum distance of $e/4$ charges is limited by the critical width of the wire where m exceeds Δ . Still, for wires of width 200 nm or wider the charges have a very small overlap and can be thought of as separate entities.

Conclusion– We introduced a realistic 1D fermion chain exhibiting three topological phases protected by chiral symmetry. Two of the phase boundaries support $\pm e/2$ zero modes while one of the phase boundaries have $\pm e$ and neutral excitations. We showed that similar topological properties are shared by quantum spin Hall wires in magnetic fields. We solved the zero energy states using combination of analytical and numerical methods and discussed how predicted properties could be realized in atomic chains and quantum spin Hall wires.

The authors would like to thank Grigory Volovik, Hans Hansson and Jens Bardarson for valuable discussions. This work was supported by Academy of Finland (T.O.) and ERC Grant No. 240362-Heatronics (J.I.V.).

* Correspondence to teemuo@boojum.hut.fi

- [1] C. L. Kane and E. J. Mele, Phys. Rev. Lett. **95**, 146802 (2005); C. L. Kane and E. J. Mele, Phys. Rev. Lett. **95**, 226801 (2005).
- [2] B. A. Bernevig, T. L. Hughes, and S.-C. Zhang, Science **314**, 1757 (2006).
- [3] C. L. Kane and M. Z. Hasan, Rev. Mod. Phys. **82**, 3045 (2010); X.-L. Qi and S.-C. Zhang, arXiv:1008.2026.
- [4] A. P. Schnyder, S. Ryu, A. Furusaki, and A. W. W. Ludwig, Phys. Rev. B **78**, 195125 (2008); S. Ryu, A. P. Schnyder, A. Furusaki, and A. W. W. Ludwig, New J. Phys **12**, 065010 (2010).
- [5] R. M. Lutchyn, J. D. Sau, and S. Das Sarma, Phys. Rev. Lett. **105**, 077001 (2010).
- [6] Y. Oreg, G. Refael, and F. von Oppen, Phys. Rev. Lett. **105**, 177002 (2010).
- [7] J. Alicea *et al.*, Nature Phys. **7**, 412 (2011).
- [8] W. P. Su, J. R. Schrieffer, and A. J. Heeger, Phys. Rev. Lett. **42**, 1698 (1979); W. P. Su, J. R. Schrieffer, and A. J. Heeger, Phys. Rev. B **22**, 2099 (1980).
- [9] V. Gurarie, Phys. Rev. B **83**, 085426 (2011).
- [10] G. E. Volovik, *The Universe in a Helium Droplet* (Clarendon Press, Oxford 2003).
- [11] R. Jackiw and C. Rebbi, Phys. Rev. D **13**, 3398 (1976).

- [12] J. I. Väyrynen and G. E. Volovik, JETP Lett. **93**, 344 (2011).
- [13] R. H. M. Smit, C. Untiedt, G. Rubio-Bollinger, R. C. Segers, and J. M. van Ruitenbeek, Phys. Rev. Lett. **91**, 076805 (2003).
- [14] L. Fernandez-Seivane, V. M. Garcia-Suarez, and J. Ferrer, Phys. Rev. B **75**, 075415 (2007);
- [15] X.-L. Qi, T. L. Hughes, and S.-C. Zhang, Nature Phys. **4**, 273 (2008).
- [16] B. Zhou, H.-Z. Lu, R.-L. Chu, S.-Q. Shen, and Q. Niu, Phys. Rev. Lett. **101**, 246807 (2008).